Numerical Investigation of Methane/Oxygen and Methane/LOX Counter-flowing Spray Flames at Elevated Pressure

D. Urzica and E. Gutheil*
Interdisciplinary Center for Scientific Computing, Heidelberg University
Im Neuenheimer Feld 368, 69120 Heidelberg, Germany

Abstract

In liquid rocket propulsion systems, methane and kerosene have been discussed as alternative fuels to hydrogen because of their high energy content. Methane has some advantages compared to kerosene because of its cleaner burning characteristics. The present study concerns the numerical investigation of laminar methane/air and methane/oxygen flames where different mixtures of nitrogen and oxygen in the oxidizer stream are studied. Moreover, liquid oxygen (LOX) spray flames with carrier gas methane against a methane stream are investigated in the counterflow configuration. These structures may be used in (spray) flamelet computations or flamelet generated manifolds for the simulation of turbulent combustion. The governing two-dimensional gas-phase equations are transformed into one-dimensional equations using a similarity transformation. For the LOX, a standard discrete droplet model is used. The numerical simulation concerns the axi-symmetric configuration with an adaptive numerical grid for the gas phase. Detailed models of all relevant processes are employed; in particular, a detailed chemical reaction mechanism is used which comprises 35 species involving 294 elementary reactions. The thermodynamic data for CH_4 and O_2 below 300K are implemented for normal and elevated pressures for cryogenic methane/LOX combustion. For the CH_4/air and an oxygenated flame, the present results are compared with both experimental and computational results from the literature. The CH_4/O_2 flame is studied for elevated pressures up to 2MPa. Extinction conditions are evaluated for use in future turbulent flamelet computations. It is shown that oxygen dilution, pressure, and strain rate have a pronounced effect on the flame structure and extinction conditions. The combustion of methane/LOX under cryogenic conditions has a pronounced effect of the liquid phase on gas temperature. After initial cooling of the gas phase due to droplet evaporation, the flame temperature is considerably higher compared to pure gas phase combustion.

Introduction

The understanding of physical and chemical processes occurring in many applications in sciences and engineering is important to ensure stability and efficiency of their performance. Examples are the combustion process in direct-injection engines, gas turbine combustors, and liquid rocket propulsion systems. The present study aims to contribute to an improved understanding of methane/oxygen and methane/LOX (liquid oxygen) combustion compared to the hydrogen/oxygen system.

In the recent years, studies have been done for the use of methane (CH_4) as an alternative fuel to hydrogen in liquid rocket propulsion systems [1-9]. The so-called 'green propellant' has become attractive because of its limited effect on environment compared to other hydrocarbons. Moreover, it has several advantages compared to hydrogen such as safety in transport and storage as well as high energy content. Currently, there are two major research groups in Europe that are carrying out experiments in order to investigate the CH_4/O_2 and methane/LOX flames, namely, ONERA in France and DLR Lampoldshausen in Germany. Both, ONERA's Mascotte test facility [2] and DLR's M3 [7], which initially were developed for experimental investigations of liquid oxygen/gaseous hydrogen combustion (LOX/H_2), have been modified to allow for the study of methane/LOX. In the experiments, pressure ranges from 0.1 to 5.5MPa, the injection temperature for LOX is 85K and for liquid CH_4 it is 125K, hence both temperatures are cryogenic. A recent study [3] has considered fuel rich conditions. Candel et al. [4] studied the flame structure of both methane/LOX and LOX/H_2 in the transcritical range for pressures between 0.1 to 7MPa and a subcritical injection temperature of liquid oxygen. Combustion of cryogenic oxygen and methane injected at pressures between 4.5 and 6MPa was investigated experimentally in [5]. The coaxial injector delivered oxygen at a temperature of 85K and methane at a temperature of 120K or 288K. Stabilization of flames formed by cryogenic liquid oxy-

*Corresponding author, e-mail: gutheil@iwr.uni-heidelberg.de

gen/gaseous hydrogen or methane was investigated through planar laser induced fluorescence (PLIF) of OH [6]. In the LOX/GH_2 experiments, injection conditions were trans-critical, since the chamber pressure (6.3MPa) was above the critical value but the temperature (80K) was below the critical value for oxygen. In the LOX/GCH_4 experiments, the chamber pressure (2MPa) and LOX injection temperature (80K) were below critical values.

In the DLR experiments [7], a comparison between spray combustion for coaxially injected methane/LOX and LOX/H_2 at similar injection conditions was performed where the Weber number and the momentum flux ratio were varying. In [8], experimental investigations on the development of methane/LOX flames, especially ignition and flame stabilization – strongly coupled with the distribution of liquid oxygen phase before and after the occurrence of ignition, were carried out. Yang et al. [9] experimentally investigated cryogenic reactive coaxial sprays with oxygen and hydrogen or methane in order to determine if concepts from LOX/H_2 injector design could be transferred to LOx/CH_4. The experimental study of the ignition and flame stabilization of a gaseous methane/oxygen jet for different configurations and injector conditions is described by Pauly [10]. In the present study, the numerical investigation of laminar CH_4/O_2 as well as methane/LOX flames in the counterflow configuration is performed in order to obtain a flamelet library for turbulent combustion and to investigate principal differences between the methane/LOX and the LOX/H_2 systems.

Laminar CH_4/air gas flames in the counterflow configuration are studied extensively in the literature. Several authors [1, 11, 12] studied the behavior of laminar CH_4/air flames in counterflow configurations at different conditions using different chemical reaction mechanisms. For instance, Chelliah *et al.* [1] present numerical results for laminar CH_4/air diffusion flames using a starting kinetic mechanism, a reduced 5-step mechanism and a 4-step mechanism are presented and the results at extinction are compared with experimental results. Du and Axelbaum [11] investigated the extinction strain rate of CH_4 - O_2 - N_2 flames using a 58-step C_1 mechanism, moreover, experimental studies were performed. Sohn *et al.* [12] numerically investigated the flame structure, extinction characteristics and nitric oxide (NO) formation in diffusion flames at various pressures in the axi-symmetric counterflow configuration. The chemical reaction mechanism used here was GRI 2.11 including NOX reactions. Other authors, [13-16] specifically studied the effect of enriched oxygen flames. For example, Cheng *et al.* [13,14] investigated oxygen-enhanced methane counterflow flames through optical diagnostics and numerical simulations. The effect of strain rate and the influence of oxygen concentration in the oxidizer stream on the flame structure were studied for nitrogen-diluted methane flames (20% CH_4 and 80% N_2). The strain rate varies from 60 to 168s^{-1} while in the oxidizer stream, the nitrogen in air is replaced by oxygen ranging from 23% O_2 to 100% O_2. For the simulations, the GRI 3.0 chemical kinetic mechanism was used. Beltrame *et al.* [16] investigated soot formation in enriched oxygen counterflow for methane-oxygen diffusion flames. It was found that soot formation in methane flames was enhanced by oxygen enrichment. With increase of the oxygen in the oxidizer stream, the soot zone narrowed and shifted towards the stagnation plane. An extension of the GRI 2.11 mechanism including chemical reactions with species up to C_6, and thus consisting of 365 reactions among 62 chemical species was used. Naik *et al.* [15] present a soot map separating non-soot from soot regions for laminar counterflow methane-oxygen-nitrogen diffusion flames at atmospheric pressure. Soot formation was studied at a constant strain rate of 20s^{-1} as a function of the methane content ranging from 25% to 100% in nitrogen directed against a stream consisting of oxygen diluted in nitrogen ranging from 35% to 100%.

The purpose of the present paper is the numerical investigation of pure CH_4/O_2 and CH_4/air flames in the counterflow configuration at normal and elevated pressures and evaluation of their extinction conditions for use in turbulent flamelet computations. Moreover, the nitrogen/oxygen ratio is varied. Properties of methane at cryogenic inlet conditions are considered which are typical for liquid rocket propulsion systems. These properties are parameterized for use in methane/LOX computations. A representative methane/LOX flame and its characteristics are presented. In the following, a short overview of the present mathematical model is given. Flame structures for CH_4/O_2 and CH_4/air and methane/LOX counterflow configuration are then presented and discussed.

Mathematical Model

An axi-symmetric counterflow configuration is considered, where either gaseous or liquid fuel may be fed against oxidizer, hot products and inert gas, in any combination, from each side of the stagnation plane [17,18,20-22]. The mathematical model is based on Eulerian/Lagrangian formulation of non-dimensional equations [17,18], which are obtained using a similarity transformation for the gas phase transforming the two-dimensional equations into a one-dimensional system. The gas-phase model includes detailed transport as well as a detailed chemical reaction mechanism [23] for the methane/air system. It consists of 294 elementary reactions among 35 species.

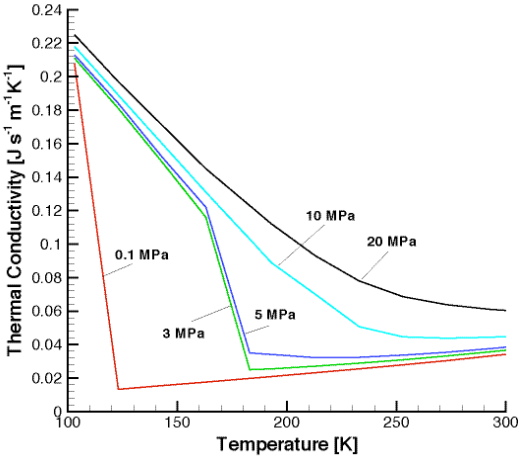

Figure 1. Pressure and temperature dependence of thermal conductivity for methane in the temperature range of 100≤T≤300K.

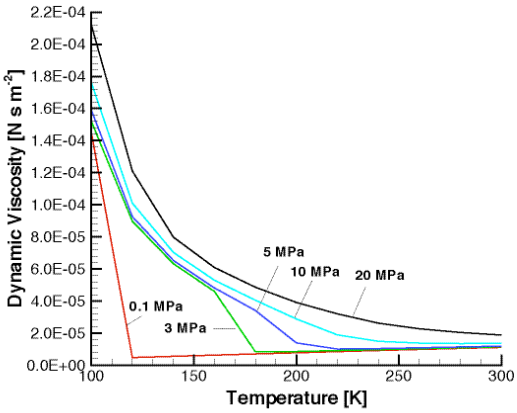

Figure 2. Pressure and temperature dependence of dynamic viscosity for methane in the temperature range of 100≤T≤300K.

The gas phase transport coefficients are computed from NASA polynomials, which cover the temperature range between 300 and 5000K. For the computation of flames under cryogenic condition, the set of physical properties must be extended for the temperature range between 100 and 300K and for pressures up to 20MPa, which was achieved using the data from the JSME tables [24].

Figures 1 and 2 show thermal conductivity (Fig. 1) and dynamic viscosity (Fig. 2) of methane for pressures between 0.1 and 20MPa and cryogenic temperatures for use in liquid oxygen/methane spray flames. In Figure 1 and Figure 2, a strong dependence of pressure and temperature on thermal conductivity and dynamic viscosity can be observed, and an extrapolation of NASA polynomials is not permitted. A more detailed description of the model may be found in the literature [17,18,20-22,29].

Previous studies have shown that the liquid phase plays a stronger role in characterizing both, the laminar and turbulent flames and, thus, may not be neglected [26-28]. The chemical reaction terms cause the system of conservation equations to be strongly non-linear and stiff. The system of equations is solved using a numerical scheme described in [17,18,20-22]. For the solution of the gas phase equations, an adaptive grid is used. The verification of the mathematical model and mechanism is achieved through comparison of the present results for CH_4/air and $CH_4/N_2/O_2$ flames with results from the literature [1,25].

Results and Discussion

Numerical results for CH_4/air, CH_4/O_2, and methane/LOX flames are presented. For gas pure gas flames, different mixture ratios of nitrogen and oxygen are presented and discussed. In the following presentations, pure fuel enters from the left-hand side of the counterflow configuration and the oxygen/nitrogen mixtures are directed against the fuel stream. First, results of the CH_4/air flame are compared with results from the literature [1,11,12,25]. In [1,25], numerical results for CH_4/air diffusion flame were computed using a detailed starting kinetic mechanism, a reduced 5-step mechanism and a 4-step mechanism. The starting mechanism was a skeletal C_1 mechanism including 39 reactions among 17 species. The strain rates at the fuel side ranged from $300s^{-1}$ to extinction for standard condition. The extinction strain rates were 518, 561, and $547s^{-1}$, for the starting kinetic mechanism, 5-step and the 4-step mechanism, respectively [1]. The extinction temperature is approximately 1800K. Du and Axelbaum [11] investigated the extinction strain rate for CH_4-N_2-O_2 diffusion flames using both numerical and experimental methods. Their simulations are based on a 58-step C_1 mechanism and an axi-symmetric configuration with standard boundary conditions resulting in an extinction strain rate of $494s^{-1}$ and an extinction temperature of 1770K, while the experimental extinction strain rate was $375s^{-1}$. Sohn *et al.* [12] studied CH_4/air flames using an axi-symmetric counterflow configuration and GRI 2.11 reaction mechanism including NOX reactions. Using the same boundary conditions as mentioned above, this study led to the extinction strain rate of about $300s^{-1}$ and an extinction temperature about 1700K.

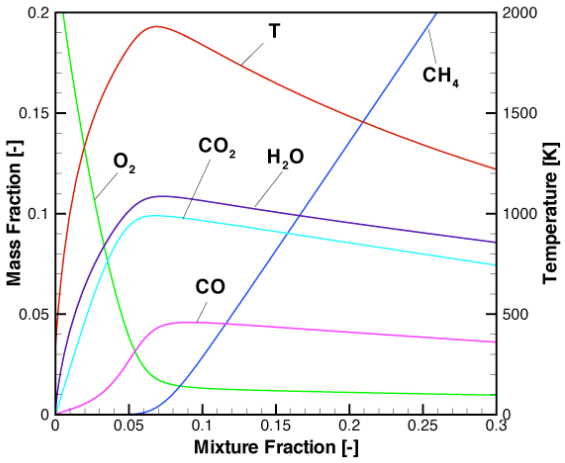

Figure 3. Profiles of temperature and mass fractions of major species for a CH_4/air flame at standard conditions for a fuel-side strain rate of $300s^{-1}$.

In the present study, a comparison of the CH_4/air flame at standard conditions and a fuel-side strain rate of $300s^{-1}$ is computed for comparison with results from the literature [1,11]. Figure 3 show profiles of some relevant species also reported by Chelliah *et al.* [1] and an excellent agreement is observed. However, the present simulations yield an extinction strain rate at the fuel side of $380s^{-1}$, which is considerably lower that the result obtained by by Chelliah *et al.* [1]. The present value, however, is very close to the experimental value of $375s^{-1}$ obtained by Du and Axelbaum [11]. Sohn *et al.* [12] report and extinction strain rate of about $300s^{-1}$ using the GRI 2.11 mechanism. The major difference in all models is the chemical reaction mechanism. The present mechanism includes C_2 reactions [23], which are neglected in Refs. [1,11,12]. In stoichiometric CH_4/air flames, the recombination path consumes about 20-30% of the CH_3 radical [23] and therefore, the present mechanism includes these reaction rates. The discrepancies between the present simulations (Fig. 3) and the results in the literature [1,11,12] are contributed to the different chemical reaction mechanisms.

The extinction temperature reported by Chelliah *et al.* [1] is approximately 1800K whereas the present computations yield a value of 1874K. The numerically obtained extinction temperature in [11] is 1770K. Other study on CH_4/air flames by Sohn *et al.* [12], using the GRI 2.11 reaction mechanism including NOX reactions results in an extinction temperature of 1700K. The comparison shows that there is still some work to be done with respect to evaluation of correct chemical kinetic rate data.

Next, laminar CH_4/O_2 flames are investigated. This is achieved through successive replacement of nitrogen by oxygen in the air stream opposing the methane flow. For a molar mixture of 68% O_2 and 32% nitrogen, there are results by Beltrame *et al.* [16]. They use an extended GRI-2.11 chemical kinetic mechanism up to C_6 for standard conditions, and the strain rate on the fuel side of the configuration is $20s^{-1}$. Figure 4 shows the present results of the outer flame structure of this configuration using the Warnatz mechanism for the same conditions. They are in very good agreement with the results of Beltrame *et al.* [16]. For instance, in [16] the peak flame temperature is about 2800K, peak values of H_2O and H_2 mole fractions is about 0.38 and 0.2 while in the present results, the peak flame temperature is 2871K and the corresponding peak values of H_2O and H_2 are 0.38 and 0.21. Thus, the present model and the chemical mechanism are suitable to represent relevant results in the literature.

Removal of nitrogen from the air stream is continued until pure methane/oxygen flames are obtained. Figure 5 shows the maximum temperature and the mass fractions of species CH_3, CO, O, OH, C_2H_2, C_2H_6, H as well as CH_2O as a function of the oxygen mass fraction at a strain rate of $100s^{-1}$. The oxygen mass fraction starts from 0.233 (CH_4/air) to unity (pure O_2). With an increase of oxygen content in the oxidizing gas stream, maximum flame temperature increases substantially from 1874K to 2965K. The maximum mass fraction of the major species plotted in Figure 5 increases non-linearly as nitrogen is removed from the system. At the same time, formaldehyde is decreased with nitrogen removal.

The pollutants and soot formation are of particular interest. The detailed chemical reaction mechanism used here is favorably enabled to predict formation of species such as CO and CH_2O as well as soot precursors such as acetylene, C_2H_2. Maximum mass fraction of carbon monoxide and acetylene increases by a factor of about 10 as nitrogen is removed. The maximum mass fraction of other species such as CH_2O is decreasing as nitrogen is removed, however, the reduction is much smaller.

Figure 6 shows the comparison of the outer flame structure of the CH_4/air (black) and the CH_4/O_2 (red) flames at the strain rates near extinction and standard conditions. The inset figure shows an enlarged view of the CH_4/O_2 flame for the same conditions. With replacement of nitrogen by oxygen, the flame thickness decreases dramatically by about a factor of seven. This is due to the fact that the damping of chemical reactions by nitrogen is removed with replacement of nitrogen by oxygen leading to enhanced chemical reactions. They are accompanied by a pronounced increase of flame temperature, which again leads to higher values of mass fraction for the major species in the chemical reaction system.

It can be observed that the flame resides on the oxidizer side of the flame, which is typical for gas flames of this type. For the methane/oxygen flame, however, the flame is shifted towards the stagnation plane. The extinction strain rate for CH_4/air flame is $380s^{-1}$, and the corresponding value for the CH_4/O_2 flame is $46{,}750s^{-1}$. The extinction strain rate of CH_4/O_2 at 0.9MPa is found to be $338{,}500s^{-1}$ with an extinction temperature of 2662K versus 2,490K for the CH_4/O_2 flame at 0.1MPa. For 2.0MPa, the corresponding values are $667{,}500s^{-1}$ and 2801K. As extinction is approached, the temperature drop with increased strain is striking. Figure 6 shows that all the major species attain higher maximum values of all mass fractions compared to the CH_4/air flame as a consequence of the elevated flame temperature.

Figure 7 shows extinction strain rates and maximum flame temperature for various configurations. Besides the flames discussed already, methane/oxygen flames at elevated pressures are displayed which are relevant for liquid rocket propulsion applications for pressures 0.1, 0.9, and 2MPa. Pressure increase leads to increased flame stability and to increased extinction strain rates and temperatures as anticipated.

Figure 8 displays the outer flame structure of a monodisperse methane/LOX spray flame at strain rate 100/s, pressure 0.1MPa, and initial droplets radius of 25µm. The oxygen droplets vaporize well before they reach the stag-

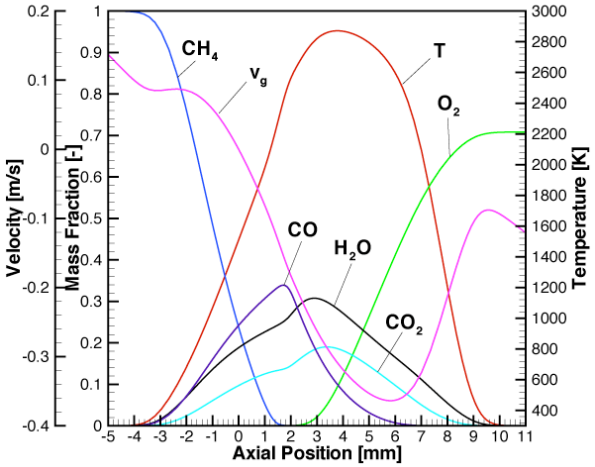

Figure 4. Profiles of temperature and mass fractions of CH_4, O_2, H_2O, CO_2 and CO for a $CH_4/O_2/N_2$ flame at a fuel-side strain rate of $20s^{-1}$.

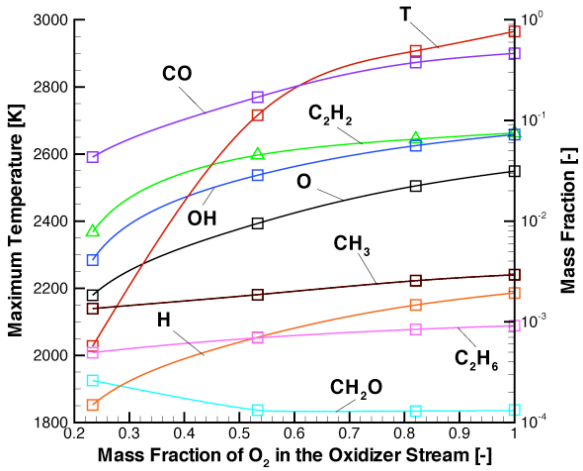

Figure 5. Maximum flame temperature and mass fraction of various species with increase of oxygen content in the oxidizer stream, strain rate $100s^{-1}$.

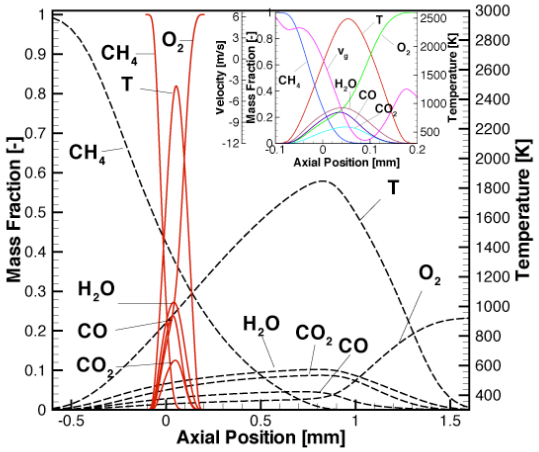

Figure 6. Profiles of temperature and mass fractions of CH_4, O_2, H_2O, CO_2 and CO of a CH_4/air (black) and a CH_4/O_2 (red) flame at extinction.

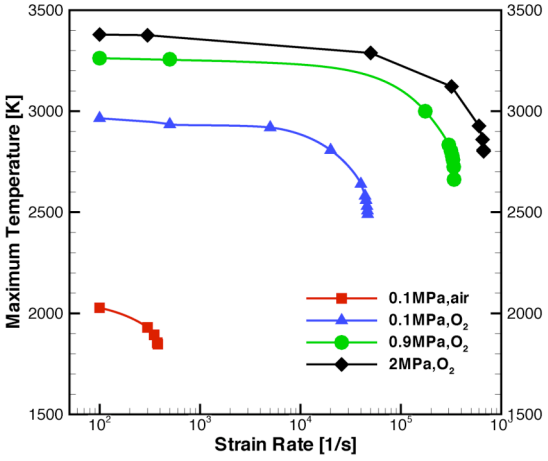

Figure 7. Maximum flame temperature for strain rates up to extinction.

nation plane. The maximum peak temperature in the methane/LOX flame is higher in comparison with the CH_4/O_2 flame, because the spray flame is leaner than the gas flame due to LOX addition enhancing combustion for the methane/LOX spray flame. The figure also shows that there is pronounced flow separation in the regime where droplets are present. Thus, the liquid phase pronouncedly affects the flame structure.

Summary and Conclusions

The study provides flame structures of methane/oxygen flames in the counterflow configuration. Both extinction strain rates and maximum flame temperature are presented for inclusion into future flamelet computations of turbulent reactive flows. Computations of methane/LOX flames show that the liquid phase has pronounced impact on the laminar flame structure and its consideration is inevitable in the prediction of reliable flame structures.

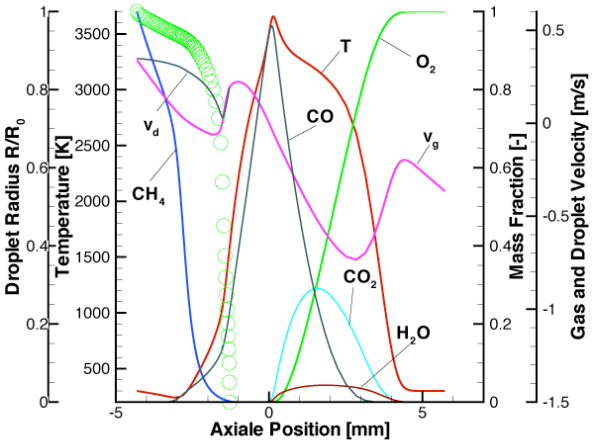

Figure 8. Profiles of temperature and of mass fractions of H_2O, CO_2 and CO for the methane/LOX spray flame, strain rate $100s^{-1}$, pressure 0.1MPa, initial droplet radius 25µm and initial velocities 0.4m/s.

Acknowledgement

The authors acknowledge financial support of Deutsche Forschungsgemeinschaft (DFG) through SFB568.

References

1. Chelliah, H.K., Seshadri, K., Law. C.K. in: Reduced Kinetic Mechanisms for Applications in Combustion Systems. Springer, 1993.
2. Zurbach, S., Thomas, J.L., Vuillermoz, P., Vingert, L. and Habiballah, M., *AIAA* 38, 2002.
3. Zurbach, S., Thomas, J.L., Verplancke, C., Vingert, L. and Habiballah, M., *AIAA* 39, 2003.
4. Candel, S., Juniper, M., Singla, G., Scouflaire, P. and Rolon, C., *Combust. Sci. and Tech.* 178, 161–192, 2006.
5. Singla, G., Scouflaire, P., Rolon, C. and Candel, S., *Proc. Combust. Inst.* 30, 2921–2928, 2005.
6. Singla, G., Scouflaire, P., Rolon, C. and Candel, S.: *Proc. Combust. Inst.* 31, 2215–2222, 2007.
7. Cuoco, F., Yang, B. and Oschwald, M., *ISTS* 24, 2004.
8. Cuoco, F., Yang, B., Bruno, C., Haidn, O.J. and Oschwald, M., *AIAA* 40, 2004.
9. Yang, B., Cuoco, F. and Oschwald, M., *J. of Propulsion and Power* 23(4), 763–771, 2007.
10. Pauly, C., PhD thesis, *DLR, Lampoldshausen*, 2006.
11. Du, J. and Axelbaum, L., *Proc. Combust. Inst.* 26, 1137–1142, 1996.
12. Sohn, C.H., Jeong, I.M. and Chung, S.H., *Combust. Flame* 130, 83–93, 2002.
13. Cheng, Z., Wehrmeyer, A. and Pitz, J.R.W., *Combust. Sci. and Tech.*, (178), 2145–2163, 2006.
14. Cheng, Z.; Wehrmeyer, A. and Pitz, J.R.W., *AIAA* 42, Reno, Nevada, 2004.
15. Naik, S.V., Laurendeau, N.M., Cooke, J.A. and Smooke, M.D., *Combust. Sci. and Tech*. 175, 1165–1167, 2003.
16. Beltrame, A., Porshnev, P., Merchan-Merchan, W., Saveliev, A., Fridman, A, Kennedy, L.A., Petrova, O., Zhdanok, S., Amouri, F. and Charon, O., *Combust. Flame* 124, 295–310, 2001.
17. Continillo, G. and Sirignano, W.A., *Combust. Flame* 81, 325-340, 1990.
18. Gutheil, E. and Sirignano, W.A., *Combust. Flame* 113, 92-105, 1998.
19. Abramzon, G. and Sirignano, W.A., *Int. J. Heat Mass Transfer*, 9, 1605-1618, 1989.
20. Schlotz, D. and Gutheil, E., Combust. *Sci. and Tech*. 158, 195210, 2000.
21. Gutheil, E., *Combustion Theory and Modelling* 5(2), 131-145, 2001.
22. Gutheil, E., *Progress in Computational Fluid Dynamics*, 5(7), 414-419, 2005.
23. Warnatz, J., Maas, U. and Dibble, R.W., *Springer, Berlin Heidelberg, New York*, 2nd Edition, 1999.
24. J. S. M. E.: *Data Book, Thermophysical Properties of Fluids*. 1983.
25. Bollig, M., Linan, A., Sanchez, A.L. and Williams, W.A., *Combust. Inst.* 27, 595 - 603, 1998.
26. Peters, N., *K. Bray, Ed., Lecture Notes in Physics, Springer*, 2006.
27. Hollmann, C. and Gutheil, E., *Proc. Combust. Inst.* 26, Vol. 1, 1731-1738, 1996.
28. Hollmann, C. and Gutheil, E, *Combust. Sci. and Tech*. 135, 1(6), 175, 1998.
29. Urzica, D. and Gutheil, E., *Z. Phys. Chem.* 223, 2009, in press.